Frontiers of Information Technology & Electronic Engineering
www.jzus.zju.edu.cn; engineering.cae.cn; www.springerlink.com
ISSN 2095-9184 (print); ISSN 2095-9230 (online)
E-mail: jzus@zju.edu.cn

Differential coupling contributes to synchronization via a capacitor connection between chaotic circuits*

Yu-meng XU[1], Zhao YAO[1], Aatef HOBINY[2], Jun MA[†‡1]

[1]*Department of Physics, Lanzhou University of Technology, Lanzhou 730050, China*

[2]*NAAM-Research Group, Department of Mathematics, King Abdulaziz University, Jeddah 21589, Saudi Arabia*

[†]E-mail: hyperchaos@163.com

Received Aug. 21, 2018; Revision accepted Oct. 22, 2018; Crosschecked Jan. 14, 2019; Published online Jan. 23, 2019

Abstract: Nonlinear oscillators and circuits can be coupled to reach synchronization and consensus. The occurrence of complete synchronization means that all oscillators can maintain the same amplitude and phase, and it is often detected between identical oscillators. However, phase synchronization means that the coupled oscillators just keep pace in oscillation even though the amplitude of each node could be different. For dimensionless dynamical systems and oscillators, the synchronization approach depends a great deal on the selection of coupling variable and type. For nonlinear circuits, a resistor is often used to bridge the connection between two or more circuits, so voltage coupling can be activated to generate feedback on the coupled circuits. In this paper, capacitor coupling is applied between two Pikovsk-Rabinovich (PR) circuits, and electric field coupling explains the potential mechanism for differential coupling. Then symmetric coupling and cross coupling are activated to detect synchronization stability, separately. It is found that resistor-based voltage coupling via a single variable can stabilize the synchronization, and the energy flow of the controller is decreased when synchronization is realized. Furthermore, by applying appropriate intensity for the coupling capacitor, synchronization is also reached and the energy flow across the coupling capacitor is helpful in regulating the dynamical behaviors of coupled circuits, which are supported by a continuous energy exchange between capacitors and the inductor. It is also confirmed that the realization of synchronization is dependent on the selection of a coupling channel. The approach and stability of complete synchronization depend on symmetric coupling, which is activated between the same variables. Cross coupling between different variables just triggers phase synchronization. The capacitor coupling can avoid energy consumption for the case with resistor coupling, and it can also enhance the energy exchange between two coupled circuits.

Key words: Synchronization; Voltage coupling; Chaotic circuit; Capacitor coupling
https://doi.org/10.1631/FITEE.1800499 **CLC number:** O59; TN710

1 Introduction

Analog circuits can be built to detect and analyze the outputs of many nonlinear dynamical systems (Ikezi et al., 1983; Timmer et al., 2000; Kiliç et al., 2002; Hanias et al., 2006; Muthuswamy and Chua, 2010), which can generate periodic and chaotic series. For example, neural circuits (Davison and Ehlers, 2011; Adesnik et al., 2012; Ren et al., 2017; Zhang et al., 2018a) can be designed to reproduce the main dynamical properties of electrical activities in an isolated neuron and coupled neurons. The neural network of circuits can be effective in investigating the collective behaviors of a nervous system. Nonlinear analysis provides reliable methodologies for signal processing and decoding of information. The circuit equations can be described when electric devices are connected to build any oscillatory circuit according to Kirchhoff's law. Furthermore, scale transformation is applied to obtain dimensionless dynamical systems, so a reliable algorithm can be used to find numerical solutions for the variables, and

‡ Corresponding author

* Project supported by the National Natural Science Foundation of China (No. 11672122)

ORCID: Jun MA, http://orcid.org/0000-0002-6127-000X

then feasible procedures (Andrievskii and Fradkov, 2004; Nazzal and Natsheh, 2007; Schöll and Schuster, 2008; Wang et al., 2012, 2015; Guo et al., 2018) can be activated for target control.

Synchronization can be triggered when an appropriate coupling is applied between two or more agents, and it is thought of as a class of cooperation and competition via exchange of energy flow. For multi-agent systems and a network of oscillators, internal cooperation and external forcing (periodic or even noise) (Qin et al., 2014; Ma et al., 2015) can enhance the realization of consensus in dynamical behaviors such as amplitude and phase. An isolated circuit generates a finite signal in amplitude and even chaotic circuits can generate a variety of signals with frequency differences. Nonlinear circuits can be coupled to enhance the power of outputs, and synchronization based on chaotic circuits has potential applications in secure communications (Wu and Chua, 1993; Boccaletti et al., 1997; Zaher and Abu-Rezq, 2011). Some researchers regard the nervous system as a complex network of integrated circuits, and each neuron is thought of as an effective nonlinear circuit for signal processing. Electric synapses and chemical synapses (Eccles, 1982; Bennett, 1997, 2000; Kopell and Ermentrout, 2004; Song et al., 2015) play important roles in receiving and propagating signals. Gap junction coupling (Bennett, 1997; Song et al., 2015) is often used to investigate the electrical response between neurons connected with electric synapses, and even most biological researchers argue that neurons should be considered as a chemical synapse connection. Indeed, a gap junction is the same as voltage coupling via a resistor, which can consume certain energy during signal processing and propagation. As a result, the power consumption of coupling resistors can be very large when millions of neurons are connected via complex paths or links. Chemical synapse coupling (Balenzuela and García-Ojalvo, 2005; Li et al, 2007; Burić et al., 2008) depends on the diffusion of neurotransmitters, and the cost of Joule heat on the coupling resistor is removed; therefore, it provides important guidance for circuit synchronization.

It is well known that a resistor connection just generates voltage coupling and the difference between output voltages from the nonlinear circuits bridged by a resistor can induce time-varying feedback on each circuit by applying an external stimulus. Indeed, when a capacitor is used to bridge a connection between two nonlinear circuits, the outputs from each circuit can charge the plates, and the distribution of electric field in the capacitor will be changed. As a result, the exchange of field energy and charges will impose appropriate feedback on both of the coupled circuits. In this paper, two Pikovsk-Rabinovich (PR) chaotic circuits (Pikovsky and Rabinovich, 1978) are connected with a resistor and capacitor to detect when synchronization is realized for each. Symmetric coupling in the same channel and cross coupling between different channels are used to investigate the stability of synchronization.

2 Model description and method

Nonlinear electric devices are critical for building chaotic circuits. The well-known nonlinear electric devices include the negative resistor, nonlinear capacitor, nonlinear inductor, and memristor (Muthuswamy and Kokate, 2009; Buscarino et al., 2012; Budhathoki et al., 2013; Bao et al., 2016, 2017; Zhang et al., 2018b). A negative resistor R requires the nonlinear dependence of voltage on current. A nonlinear capacitor means that the charges q on the plates change the voltage of the capacitor in a nonlinear relation. In sum, the main characteristic of nonlinear devices is that the change in an output variable does not follow the change in the input variable proportionally. These nonlinear electric devices can be applied to build a variety of chaotic circuits, and robust synchronization (Buscarino et al., 2009) can be further investigated between hyperchaotic circuits through experiments. For example, an autonomous and self-excited circuit (Pikovsky and Rabinovich, 1978; Pikovsky, 1981; He et al., 2003; Louodop et al., 2014) was built by Pikovsk and Rabinovich in 1978. The circuit was made of a capacitor C, a linear resistor r, an inductor L, a nonlinear resistor with negative conductance $-g$, and a tunnel diode with parasitic capacitance C_1. The circuit is illustrated in Fig. 1.

The tunneling diode can be switched on at a reverse bias and its reverse breakdown voltage is zero, while the quantum tunneling effect can generate a region of negative resistance under a forward bias. Fig. 2 shows the voltage-current (U-I) curve of this tunneling diode.

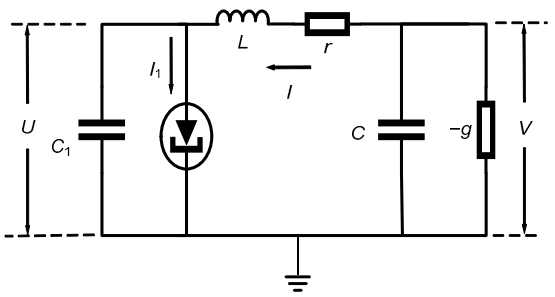

Fig. 1 Schematic of a Pikovsk-Rabinovich (PR) circuit, a self-excited oscillator

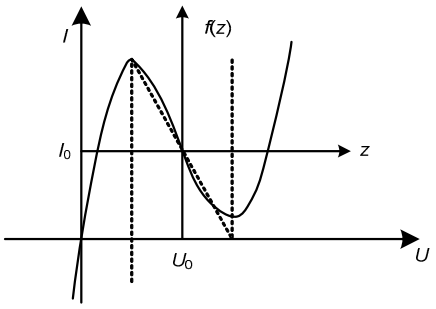

Fig. 2 *I-U* characteristic of the tunnel diode
The output voltage for capacitor C_1 is denoted as U, while V represents the voltage for negative conductance. I is the current across inductor L, and I_1 describes the current across the tunnel diode, $I_1=I_0+I_0[(U/U_0-1)^3-(U/U_0-1)]$

According to the physical Kirchhoff law, the circuit equations for Fig. 1 can be approached as

$$\begin{cases} V-U=rI+L\dfrac{\mathrm{d}I}{\mathrm{d}t}, \\ -I=C\dfrac{\mathrm{d}V}{\mathrm{d}t}-gV, \\ I=I_1+C_1\dfrac{\mathrm{d}U}{\mathrm{d}t}. \end{cases} \tag{1}$$

For further dynamical analysis and numerical studies, scale transformation is proposed to obtain a dimensionless dynamical system. It requires the variable transformation as follows:

$$\begin{cases} x=\dfrac{I}{I_0}-1,\ y=\dfrac{V-Ir-U_0}{\omega LI_0},\ z=\dfrac{U}{U_0}-1,\ \tau=t\omega, \\ \omega=\sqrt{\dfrac{1-gr}{LC}},\ \delta=\dfrac{U_0}{\omega I_0 L},\ 2\gamma=\dfrac{gL-rC}{\omega LC}, \\ \alpha=\dfrac{rU_0}{\omega^2L^2I_0},\ \beta=-1+\dfrac{gU_0}{\omega^2I_0LC},\ \mu=\dfrac{I_0}{\omega C_1U_0}. \end{cases} \tag{2}$$

As a result, the dimensionless dynamical system can be described by three-variable ordinary differential equations (ODEs) as follows:

$$\begin{cases} \dfrac{\mathrm{d}x}{\mathrm{d}\tau}=y-\delta z, \\ \dfrac{\mathrm{d}y}{\mathrm{d}\tau}=-x+2\gamma y+\alpha z+\beta, \\ \dfrac{\mathrm{d}z}{\mathrm{d}\tau}=\mu(x+z-z^3). \end{cases} \tag{3}$$

The dynamics (3) can be investigated via bifurcation analysis, and different attractors can be formed by setting appropriate parameters. For example, a chaotic series can be observed by applying the parameters as δ=0.66, γ=0.201, α=0.165, β=0, and μ=1/0.047. From a control view, the stabilization of variable y is very important for control of chaos. In the case of synchronization problems, two identical PR circuits are often coupled via different channels or variables. The coupled circuits are plotted in Fig. 3, where X describes the coupling channel; for example, when the output ends 1-2 or 3-4 are connected, symmetric coupling is activated so that the same variables are coupled. However, cross coupling is switched on when the output ends 1-4 or 3-2 are connected so that different variables are coupled. The coupled PR circuits under bidirectional coupling can be described by

$$\begin{cases} L\dfrac{\mathrm{d}I}{\mathrm{d}t}=V-U-rI, \\ C\dfrac{\mathrm{d}V}{\mathrm{d}t}=gV-I-\lambda_1 I_X, \\ C_1\dfrac{\mathrm{d}U}{\mathrm{d}t}=I-I_1-\lambda_3 I_X, \end{cases} \quad \begin{cases} L\dfrac{\mathrm{d}\hat{I}}{\mathrm{d}t}=\hat{V}-\hat{U}-r\hat{I}, \\ C\dfrac{\mathrm{d}\hat{V}}{\mathrm{d}t}=g\hat{V}-\hat{I}+\lambda_2 I_X, \\ C_1\dfrac{\mathrm{d}\hat{U}}{\mathrm{d}t}=\hat{I}-I_1+\lambda_4 I_X, \end{cases} \tag{4}$$

where parameters λ_1, λ_2, λ_3, and λ_4 decide the on-off state for the coupling device by resetting 0 and 1. Resistor-based voltage coupling and capacitor-based current (for an electric field) coupling can be defined by

$$I_X=\begin{cases} I_g=\pm g_X(V_i-V_j), \\ I_C=\pm C_X\dfrac{\mathrm{d}(V_i-V_j)}{\mathrm{d}t}, \end{cases} \tag{5}$$

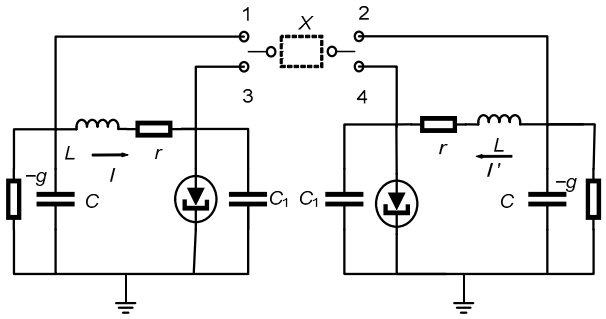

Fig. 3 Schematic of two PR circuits under different coupling channels and styles

X denotes the coupling devices, which can be resistors or capacitors. *i*=1, 3, *j*=2, 4 represent the output ends

where g_X and C_X represent the conductance of the coupling resistor and the capacitance of the coupling capacitor, respectively. The variables V_i and V_j describe the output voltage from the two PR circuits. The symbol ± selects the direction of the coupling current. The coupling current across the coupling device can trigger different forms when different output ends are connected. For the most part, we discuss the effect of resistor coupling and capacitor coupling as well when symmetric and cross coupling are considered, respectively. When the output ends 1, 2 are connected ($\lambda_1=\lambda_2=1, \lambda_3=\lambda_4=0$), the variables y, $\hat{y}$ are coupled, and the dynamical equations can be described by

$$\begin{cases} \dot{x} = y - \delta z, \\ \dot{y} = -x + 2\gamma y + \alpha z + \beta \\ \quad\quad -\left[k_1(y-\hat{y}) + k_1 \dfrac{\alpha}{\delta}(x-\hat{x}) \right], \\ \dot{z} = \mu(x + z - z^3), \\ \dot{\hat{x}} = \hat{y} - \delta \hat{z}, \\ \dot{\hat{y}} = -\hat{x} + 2\gamma \hat{y} + \alpha \hat{z} + \beta \\ \quad\quad +\left[k_1(y-\hat{y}) + k_1 \dfrac{\alpha}{\delta}(x-\hat{x}) \right], \\ \dot{\hat{z}} = \mu(\hat{x} + \hat{z} - \hat{z}^3), \end{cases} \tag{6}$$

where the coupling coefficient $k_1=g_X L^{1/2}/(C-Cgr)^{1/2}$, and the intrinsic parameters also modulate the coupling intensity. When the output ends 3, 4 are connected ($\lambda_1=\lambda_2=0$, $\lambda_3=\lambda_4=1$), the dynamical equations for the two coupled systems via resistor coupling can be described by

$$\begin{cases} \dot{x} = y - \delta z, \\ \dot{y} = -x + 2\gamma y + \alpha z + \beta, \\ \dot{z} = \mu[x + z - z^3 - k_2(z-\hat{z})], \\ \dot{\hat{x}} = \hat{y} - \delta \hat{z}, \\ \dot{\hat{y}} = -\hat{x} + 2\gamma \hat{y} + \alpha \hat{z} + \beta, \\ \dot{\hat{z}} = \mu[\hat{x} + \hat{z} - \hat{z}^3 + k_2(z-\hat{z})], \end{cases} \tag{7}$$

where the coupling coefficient $k_2=g_X U_0/I_0$, and the intrinsic parameters in the tunnel diode also give possible modulation on the coupling intensity. Eqs. (6) and (7) suggest the case for symmetric coupling. The case for cross coupling is also attractive. When the output ends 3, 2 are connected ($\lambda_3=\lambda_2=1, \lambda_1=\lambda_4=0$), the dynamical equations are given as follows:

$$\begin{cases} \dot{x} = y - \delta z, \\ \dot{y} = -x + 2\gamma y + \alpha z + \beta, \\ \dot{z} = \mu\left[x + z - z^3 \right. \\ \quad\quad \left. -\left(k_3 z - \dfrac{k_3}{\delta}\hat{y} - k_3 \dfrac{\alpha}{\delta^2}\hat{x} - k_3 \dfrac{\alpha}{\delta^2} \right) \right], \\ \dot{\hat{x}} = \hat{y} - \delta \hat{z}, \\ \dot{\hat{y}} = -\hat{x} + 2\gamma \hat{y} + \alpha \hat{z} + \beta \\ \quad\quad +\left(k_3 z - \dfrac{k_3}{\delta}\hat{y} - k_3 \dfrac{\alpha}{\delta^2}\hat{x} - k_3 \dfrac{\alpha}{\delta^2} \right), \\ \dot{\hat{z}} = \mu(\hat{x} + \hat{z} - \hat{z}^3), \end{cases} \tag{8}$$

where the coupling coefficient $k_3=g_X U_0/I_0$, and the coupling coefficients k_1, k_2, k_3 are approached under $gr \ll 1$. That is, cross coupling can be activated by connecting the output ends 3, 2 or 1, 4. For a synchronization stability approach, the error function for the coupled systems can be estimated by

$$\begin{aligned} \theta(e_x, e_y, e_z) &= \sqrt{(x-\hat{x})^2 + (y-\hat{y})^2 + (z-\hat{z})^2} \\ &= \sqrt{e_x^2 + e_y^2 + e_z^2}. \end{aligned} \tag{9}$$

Complete synchronization is stabilized when the error function decreases to zero within a finite transient period, which is dependent on the selection of the coupling coefficient and intensity as well. It is important to discuss the case in which a capacitor

coupling is activated, and then symmetric coupling and cross coupling are investigated, respectively. When the coupling capacitor is switched on between the output ends 1, 2 (λ_1=λ_2=1, λ_3=λ_4=0), the dynamical equations are confirmed as follows:

$$\begin{cases}\dot{x}=y-\delta z,\\ \dot{y}=\dfrac{k_4}{1+2k_4}\Big[-\hat{x}+2\gamma\hat{y}+\alpha\hat{z}+\beta\\ \quad+\dfrac{k_4\alpha}{\delta}(y-\hat{y})+k_4\alpha(\hat{z}-z)\Big]\\ \quad+\dfrac{1+k_4}{1+2k_4}\Big[-x+2\gamma y+\alpha z+\beta\\ \quad+\dfrac{k_4\alpha}{\delta}(\hat{y}-y)+k_4\alpha(z-\hat{z})\Big],\\ \dot{z}=\mu(x+z-z^3),\\ \dot{\hat{x}}=\hat{y}-\delta\hat{z},\\ \dot{\hat{y}}=\dfrac{k_4}{1+2k_4}\Big[-x+2\gamma y+\alpha z+\beta\\ \quad+\dfrac{k_4\alpha}{\delta}(\hat{y}-y)+k_4\alpha(z-\hat{z})\Big]\\ \quad+\dfrac{1+k_4}{1+2k_4}\Big[-\hat{x}+2\gamma\hat{y}+\alpha\hat{z}+\beta\\ \quad+\dfrac{k_4\alpha}{\delta}(y-\hat{y})+k_4\alpha(\hat{z}-z)\Big],\\ \dot{\hat{z}}=\mu(\hat{x}+\hat{z}-\hat{z}^3),\end{cases}\tag{10}$$

where the coupling coefficient k_4=C_X/C. In fact, as shown in Eq. (5), the capacitor coupling just introduces a differential modulation, and then Eq. (10) is rewritten as Eq. (11).

From the equivalent definition shown in Eq. (11), it is found that the differential error for output voltage is fed back into the coupled circuits with the gain as k_4/(2k_4+1), and the additive feedback from variable errors is also triggered when capacitor coupling is switched on. In practice, coupling coefficient k_4 and capacitance C_X can be tamed to modulate the collective responses of the coupled circuits, and then an appropriate coupling intensity could be effective in realizing synchronization. Furthermore, symmetrical coupling via a capacitor connection is considered between output ends 3, 4 (λ_1=λ_2=0, λ_3=λ_4=1), and the dynamical equations are achieved as Eq. (12).

$$\begin{cases}\dot{x}=y-\delta z,\\ \dot{y}=-x+2\gamma y+\alpha z+\beta\\ \quad+\dfrac{k_4}{1+2k_4}\Big[(-\hat{x}+2\gamma\hat{y}+\alpha\hat{z}+\beta)\\ \quad-(-x+2\gamma y+\alpha z+\beta)\Big]\\ \quad+\dfrac{k_4}{1+2k_4}\Big[\dfrac{\alpha}{\delta}(\hat{y}-y)+\alpha(z-\hat{z})\Big],\\ \dot{z}=\mu(x+z-z^3),\\ \dot{\hat{x}}=\hat{y}-\delta\hat{z},\\ \dot{\hat{y}}=-\hat{x}+2\gamma\hat{y}+\alpha\hat{z}+\beta\\ \quad+\dfrac{k_4}{1+2k_4}\Big[(-x+2\gamma y+\alpha z+\beta)\\ \quad-(-\hat{x}+2\gamma\hat{y}+\alpha\hat{z}+\beta)\Big]\\ \quad+\dfrac{k_4}{1+2k_4}\Big[\dfrac{\alpha}{\delta}(y-\hat{y})+\alpha(\hat{z}-z)\Big],\\ \dot{\hat{z}}=\mu(\hat{x}+\hat{z}-\hat{z}^3).\end{cases}\tag{11}$$

$$\begin{cases}\dot{x}=y-\delta z,\\ \dot{y}=-x+2\gamma y+\alpha z+\beta,\\ \dot{z}=\mu\Big[\dfrac{1+k_5}{1+2k_5}(x+z-z^3)+\dfrac{k_5}{1+2k_5}(\hat{x}+\hat{z}-\hat{z}^3)\Big],\\ \dot{\hat{x}}=\hat{y}-\delta\hat{z},\\ \dot{\hat{y}}=-\hat{x}+2\gamma\hat{y}+\alpha\hat{z}+\beta,\\ \dot{\hat{z}}=\mu\Big[\dfrac{1+k_5}{1+2k_5}(\hat{x}+\hat{z}-\hat{z}^3)+\dfrac{k_5}{1+2k_5}(x+z-z^3)\Big].\end{cases}\tag{12}$$

In Eq. (12) the coupling coefficient k_5=C_X/C_1. Then Eq. (12) is rewritten with an equivalent form and the differential coupling feedback can be discerned. It reads as Eq. (13) (see the next page).

It is found that differential coupling via a capacitor can be fed back into the coupled circuits under an adjustable gain k_5/(1+2k_5), and the synchronization orbits can be tamed to keep them close by applying appropriate coupling gains. Furthermore, when cross coupling via the capacitor is connected between output ends 3, 2 (λ_3=λ_2=1, λ_1=λ_4=0), it is the same case for a connection between output ends 1, 4 (λ_3=λ_2=0, λ_1=λ_4=1), and the dynamical equations can be confirmed as Eq. (14).

$$\begin{cases}\dot{x}=y-\delta z,\\ \dot{y}=-x+2\gamma y+\alpha z+\beta,\\ \dot{z}=\mu(x+z-z^3)\\ \quad+\dfrac{k_5}{1+2k_5}[\mu(\hat{x}+\hat{z}-\hat{z}^3)-\mu(x+z-z^3)],\\ \dot{\hat{x}}=\hat{y}-\delta\hat{z},\\ \dot{\hat{y}}=-\hat{x}+2\gamma\hat{y}+\alpha\hat{z}+\beta,\\ \dot{\hat{z}}=\mu(\hat{x}+\hat{z}-\hat{z}^3)\\ \quad+\dfrac{k_5}{1+2k_5}[\mu(x+z-z^3)-\mu(\hat{x}+\hat{z}-\hat{z}^3)].\end{cases}\tag{13}$$

$$\begin{cases}\dot{x}=y-\delta z,\\ \dot{y}=-x+2\gamma y+\alpha z+\beta,\\ \dot{z}=\dfrac{k_6+0.1}{k_6+1.1}\mu(x+z-z^3)\\ \quad+\dfrac{1}{k_6+1.1}\dfrac{\alpha}{\delta^2}\hat{y}-\dfrac{1}{k_6+1.1}\dfrac{\alpha}{\delta}\hat{z}\\ \quad+\dfrac{1}{k_6+1.1}\dfrac{1}{\delta}(-\hat{x}+2\gamma\hat{y}+\alpha\hat{z}+\beta),\\ \dot{\hat{x}}=\hat{y}-\delta\hat{z},\\ \dot{\hat{y}}=\dfrac{k_6+1}{k_6+1.1}(-\hat{x}+2\gamma\hat{y}+\alpha\hat{z}+\beta)\\ \quad-\dfrac{0.1}{k_6+1.1}\dfrac{\alpha}{\delta}\hat{y}+\dfrac{0.1}{k_6+1.1}\alpha\hat{z}\\ \quad+\dfrac{0.1}{k_6+1.1}\delta\mu(x+z-z^3),\\ \dot{\hat{z}}=\mu(\hat{x}+\hat{z}-\hat{z}^3).\end{cases}\tag{14}$$

In Eq. (14) the coupling coefficient $k_6=C_1/C_X$, and for simplicity, we set $C_1/C=0.1$. In the same way, coupling gain can be adjusted to find the synchronization orbits. According to our prior knowledge, bi-directional coupling supports complete synchronization between identical oscillators or systems, while phase synchronization (Parlitz et al., 1996; Neiman et al., 1999; Pikovsky et al., 2000; Fell and Axmacher, 2011; Ma et al., 2017) occurs between non-identical systems under coupling. On the other hand, sub-threshold coupling (or weak coupling) can induce phase synchronization between identical systems. The phase series can be detected by applying the Hilbert transform (Hahn, 1996) on the sampled time series for observable variables. Furthermore, the phase error can be calculated to detect the stability of phase synchronization.

$$\begin{cases}\Delta\phi(t)=\phi(t)-\hat{\phi}(t),\\ \phi(t)=\arctan\dfrac{\tilde{x}(t)}{x(t)},\ \phi'(t)=\arctan\dfrac{\tilde{\hat{x}}(t)}{\hat{x}(t)},\\ \tilde{x}(t)=-\dfrac{1}{\pi}\mathrm{PV}\int_{-\infty}^{\infty}\dfrac{x(\tau)}{t-\tau}\mathrm{d}t,\\ \tilde{\hat{x}}(t)=-\dfrac{1}{\pi}\mathrm{PV}\int_{-\infty}^{\infty}\dfrac{\hat{x}(\tau)}{t-\tau}\mathrm{d}t,\end{cases}\tag{15}$$

where PV represents the principal value of the integral, and $\phi(t)$ and $\phi'(t)$ are the phase series calculated from the time series for outputs $x(t)$ and $\hat{x}(t)$, respectively.

3 Numerical results and discussion

In this section, Matlab (ODE45) is applied to find solutions for the dynamical systems under voltage coupling and also under field coupling. The initial values for an isolated PR circuit system are selected as (0.1, 0.1, 0.1), the time step is h=0.01, the parameters are selected in the chaotic region as δ=0.66, γ=0.201, α=0.165, β=0, μ=1/0.047, and the strange attractor developed is plotted in Fig. 4.

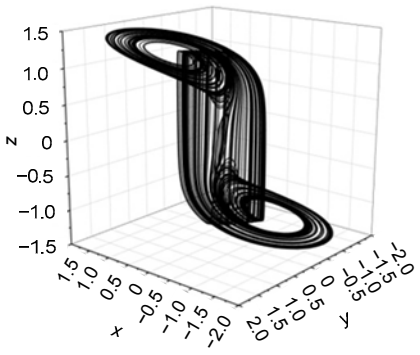

Fig. 4 Formation of a chaotic attractor in a PR circuit

The Lyapunov exponent spectrum can be calculated to find the dependence of chaos occurrence on the parameter setting. For simplicity, the maximum value of the sampled time series for variable x is estimated and the bifurcation analysis is plotted in Fig. 5.

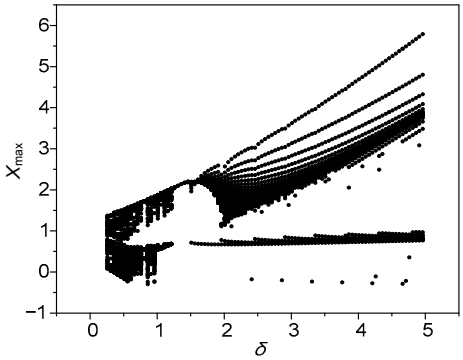

Fig. 5 Bifurcation diagram of the maximum value of variable x vs. parameter δ in the PR system

It is shown that chaos can be triggered in a large parameter region. Furthermore, some phase portraits are plotted to illustrate the dependence of the attractor profile on the parameter setting δ. The results are shown in Fig. 6.

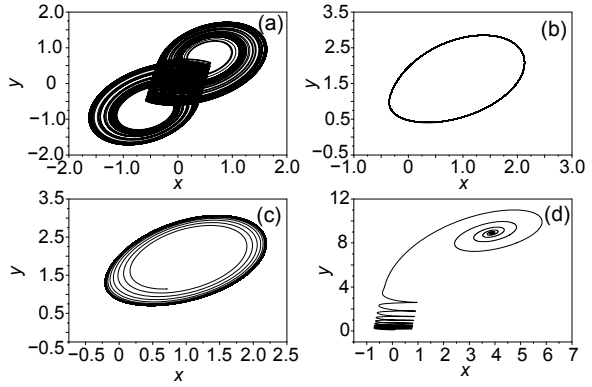

Fig. 6 Formation of attractors under different parameter values: (a) δ=0.66; (b) δ=1.35; (c) δ=1.5; (d) δ=5

In the following studies, we discuss mainly the synchronization approach and stability between chaotic PR systems. The initial values for the coupled system are selected as (0.1, 0.1, 0.1, 0.1, 0.1, 1), with the same time step of 0.01 applied. First, we investigate the case shown in Eq. (6), by which the output ends 1, 2 are connected via a resistor with conductance g_X, and the error function is estimated in Fig. 7.

It is confirmed that the error function can decrease to zero within a finite transient period; e.g., it takes about 270 time units when the coupling coefficient is selected as k_1=0.12. Furthermore, with the increase of coupling intensity, the transient period for the synchronization approach becomes shorter. Then the dependence of the maximum value of the error function is calculated under different coupling coefficients. The results are shown in Fig. 8.

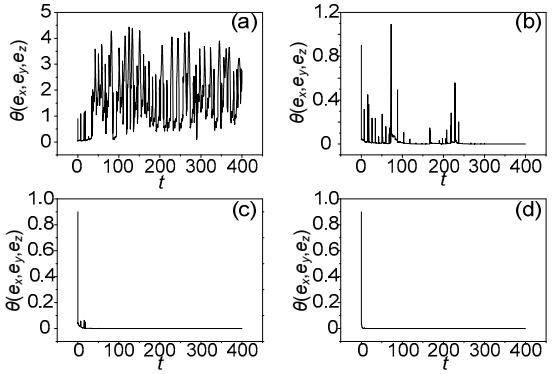

Fig. 7 Evolution of the error function via resistor coupling under the connection output ends 1, 2 for k_1=0 (a), k_1=0.12 (b), k_1=0.25 (c), and k_1=3.0 (d)

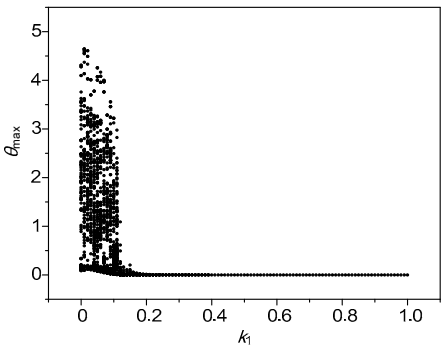

Fig. 8 Dependence of the maximum error on the coupling coefficient via resistor coupling under connection output ends 1, 2

It is shown that the maximum value of the error function can decrease to a finitely small value and that the means toward complete synchronization becomes available via resistor coupling when a single variable is used to couple the chaotic PR systems. Furthermore, the synchronization approach is detected when output ends 3, 4 are connected, for which the dynamical system under resistor coupling is defined in Eq. (7), and the results are plotted in Fig. 9.

Thus, when a coupling resistor is connected between output ends 3, 4, this complete synchronization approach becomes difficult even when the coupling coefficient is further increased. Then, we calculate the evolution of the phase series, which are

calculated using a Hilbert transform as shown in Eq. (15). The results are presented in Fig. 10.

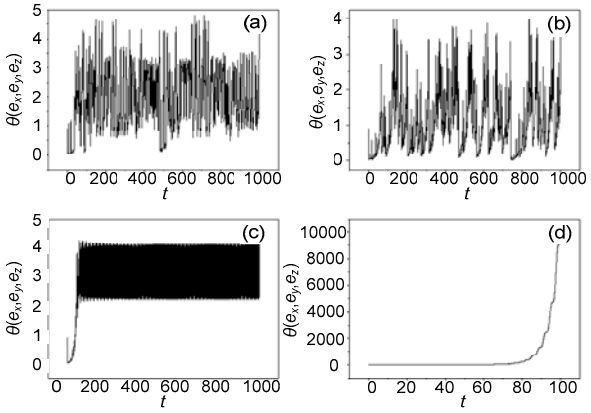

Fig. 9 Evolution of the error function via resistor coupling under connection output ends 3, 4 for k_2=0 (a), k_2=0.3 (b), k_2=0.6 (c), and k_2=1 (d)

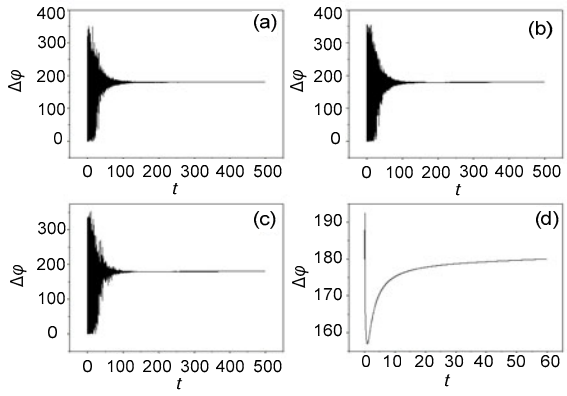

Fig. 10 Error evolution of a phase series via resistor coupling with a connection between output ends 3, 4 for k_2=0 (a), k_2=0.3 (b), k_2=0.5 (c), and k_2=1 (d)

From Fig. 10, it can be seen that anti-phase synchronization can be reached by applying an appropriate coupling coefficient when output ends 3, 4 are connected using resistor coupling. The failure of complete synchronization could be due to the fact that the coupling between the outputs from the tunnel diodes can be suppressed by the outputs from parasitic capacitance C_1 paralleled with the diode. Then, cross coupling is considered between output ends 3, 2, and the dynamical system is described by Eq. (8). The results are plotted in Fig. 11.

With the increase of the coupling coefficient for resistor connection, the maximum value for the error function just fluctuates between several finite values, and the realization of complete synchronization becomes difficult when a coupling resistor is used to bridge the connection between output ends 3, 2. Consider a clear illustration, where the evolution of the error function is calculated under different coupling coefficients, as shown in Fig. 12.

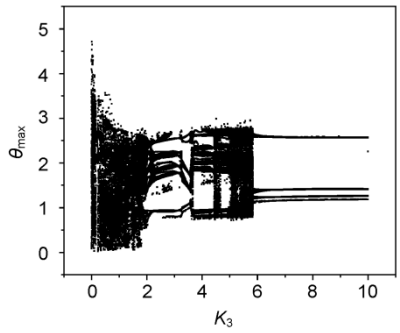

Fig. 11 Dependence of the maximum error on the coupling coefficient via resistor coupling with a connection of output ends 3, 2

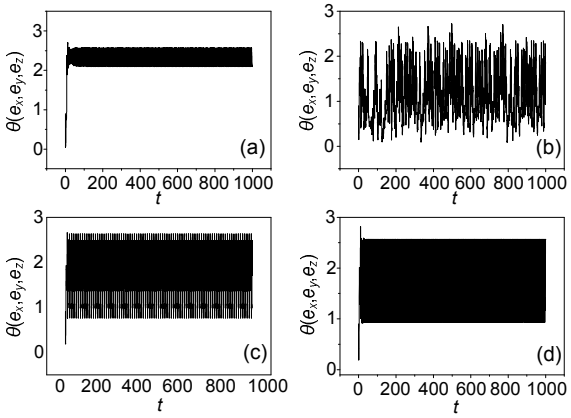

Fig. 12 Evolution of the error function via resistor coupling under connection output ends 3, 2 for k_3=0.2 (a), k_3=1.5 (b), k_3=3.5 (c), and k_3=8 (d)

The results in Fig. 12 provide evidence that cross coupling via a resistor can generate the coexistence of chaos and periodicity, and the transition from chaos to periodicity can be induced with the increase of the coupling coefficient. Furthermore, we calculate the phase series to observe the occurrence of phase synchronization, and the results are plotted in Fig. 13.

Phase synchronization can be stabilized under cross coupling when the coupling resistor bridges the connection between output ends 3, 2, and the transient

period is shortened with an increase in the coupling coefficient. As mentioned above, capacitor coupling can contribute to the transmission of energy flow between the coupled circuits. Therefore, it is important to discuss the case for capacitor coupling, as mentioned above, where the coupling capacitor is bridged to connect output ends 1, 2 and then symmetric coupling is activated. This case is described by the dynamical system as defined in Eq. (10), and the results are plotted in Fig. 14.

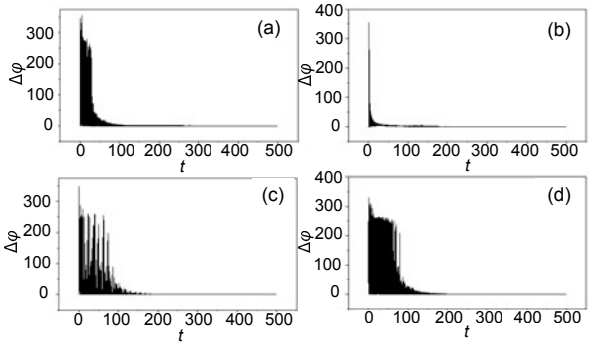

Fig. 13 Evolution of the phase error under cross coupling via a linear resistor when output ends 3, 2 are connected for k_3=0.16 (a), k_3=0.21 (b), k_3=3.2 (c), and k_3=5 (d)

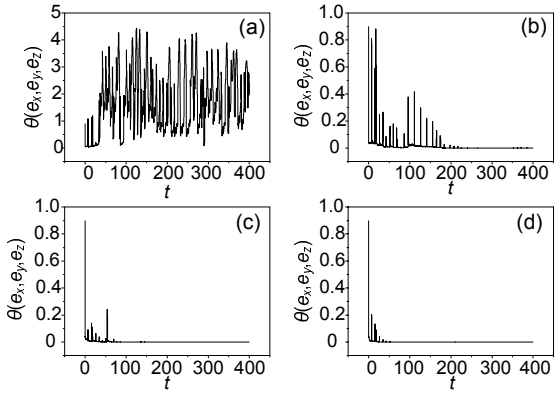

Fig. 14 Evolution of the error function via capacitor coupling under connection output ends 1, 2 for k_4=0 (a), k_4=0.23 (b), k_4=1.0 (c), and k_4=4.0 (d)

It is verified that complete synchronization between the two chaotic PR systems becomes stable when the coupling capacitor activates symmetrical coupling at the appropriate coupling coefficient, and the transient period becomes shorter with the increase of the coupling coefficient. In addition, the maximum value for the error function is estimated under different coupling coefficients, and the results are illustrated in Fig. 15.

The bifurcation diagram predicts that complete synchronization can be reached when capacitor coupling is applied with an appropriate coupling coefficient beyond the threshold of k_4~0.23. Capacitor coupling is also considered between output ends 3, 4, whose dynamical system is described by Eq. (12). The results are given in Fig. 16.

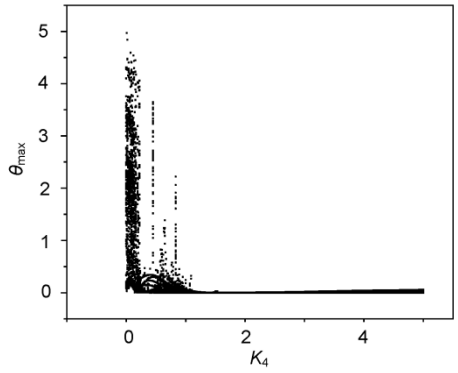

Fig. 15 Dependence of the maximum error on the coupling coefficient via capacitor coupling under connection output ends 1, 2

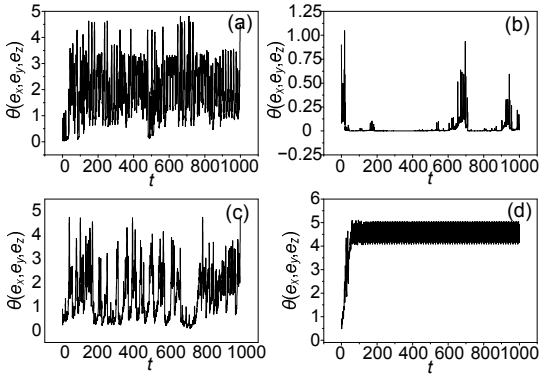

Fig. 16 Evolution of the error function via capacitor coupling under connection output ends 3, 4 for k_5=0 (a), k_5=1 (b), k_5=5 (c), and k_5=11 (d)

That is to say, complete synchronization between the two chaotic PR systems becomes difficult even if a capacitor is applied to connect output ends 3, 4. Furthermore, the phase series from the two PR systems are calculated to find the possibility of phase synchronization. The results are shown in Fig. 17.

It is found that the two chaotic PR systems can be stabilized at phase synchronization, while anti-phase synchronization is reached with a further

increase of the coupling coefficient for the coupling capacitor. It seems that capacitor coupling shows more efficiency in keeping the stability of phase synchronization and anti-phase synchronization than resistor coupling between output ends 3, 4. Finally, cross coupling via the capacitor is verified by connecting output ends 3, 2, whose dynamical system is described by Eq. (14). The results are shown in Figs. 18 and 19.

The error function between the two chaotic PR systems becomes time-varying even when the coupling coefficient for the coupling capacitor increases greatly, and extensive numerical results confirm that the profile of chaotic attractors shows distinct diversity and difference. Then the phase series are calculated to analyze the phase synchronization, and the results are plotted in Fig. 19.

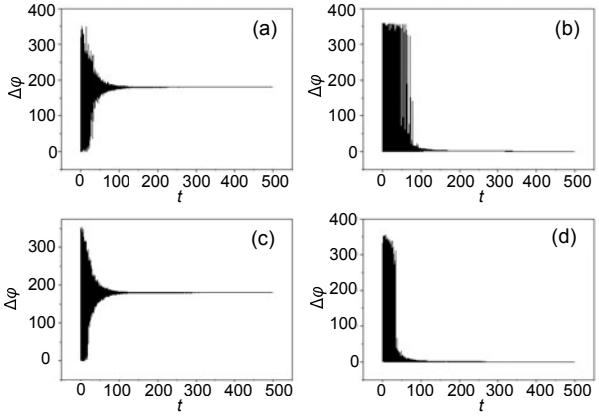

Fig. 17 Evolution of the phase error under cross coupling via a linear resistor when output ends 3, 4 are connected for k_5=0 (a), k_5=1 (b), k_5=5 (c), and k_5=7.1 (d)

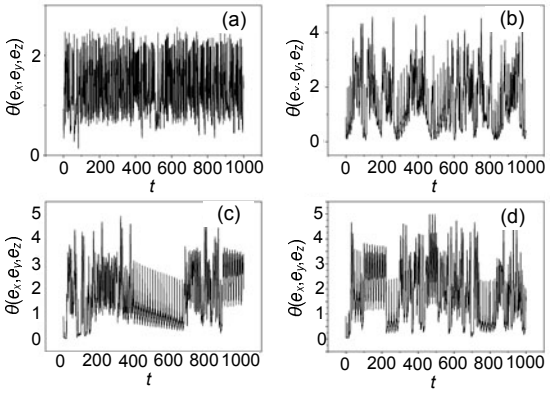

Fig. 18 Evolution of the error function via capacitor coupling under connection output ends 3, 2 for k_6=0.01 (a), k_6=0.6 (b), k_6=4 (c), and k_6=10 (d)

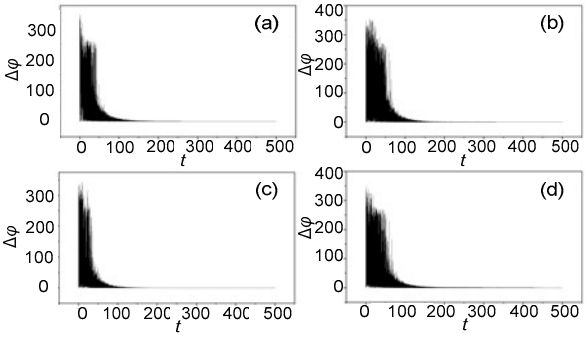

Fig. 19 Evolution of the phase error under cross coupling via a capacitor when output ends 3, 2 are connected for k_6=0.01 (a), k_6=0.6 (b), k_6=4 (c), and k_6=10 (d)

According to the previous definition for a coupling coefficient, we have $k_5=1/k_6=C_X/C_1$; as a result, the modulation and feedback from the coupling capacitor is enhanced when the coupling capacitor is endowed with a larger value and the synchronization approach becomes relaxed. When the coupling capacitor is selected with finite capacitance values, a certain transient period is needed to reach synchronization stability.

In summary, the synchronization approach depends heavily on the coupling channel and coupling type. The capacitor coupling plays the same role in realizing complete synchronization between chaotic systems, and the coupling capacitor just enhances the energy exchange of the electric field and never consumes energy while the coupling resistor has to consume a certain amount of Joule heat and energy when the coupling is activated. Complete synchronization is realized when resistor coupling or capacitor coupling is applied to connect the outputs from capacitor C in each circuit, while coupling between parasitic capacitance C_1 in the chaotic PR circuits cannot support complete synchronization other than phase synchronization. Cross coupling via a linear resistor or capacitor can induce phase synchronization. Indeed, a time-varying electric field is induced in the coupling capacitor, and energy flow is transmitted across this coupling capacitor when the coupling connection is switched on. As a result, the coupled circuits are regulated to keep pace with each other, while resistor-based voltage coupling just consumes the Joule energy to suppress nonlinear oscillations in the coupled PR circuits. This type of coupling via capacitor simply provides evidence for understanding

the well-known differential coupling control. On the other hand, a capacitor coupling builds a bridge for the exchange of field energy. For *L*-*C* (inductor and capacitor) circuits, the electric field energy is included in the capacitor while the magnetic field energy stays in the inductor. Then the field energy in the driving, response system and coupling capacitor can be described by

$$\begin{cases} H_1=\dfrac{1}{2}CV^2+\dfrac{1}{2}C_1U^2+\dfrac{1}{2}LI^2, \\ H_2=\dfrac{1}{2}C\hat{V}^2+\dfrac{1}{2}C_1\hat{U}^2+\dfrac{1}{2}L\hat{I}^2, \\ H_{C_X}=\dfrac{1}{2}C_X(V-\hat{V})^2, \text{ output ends 1, 2 are connected,} \\ H_{C_X}=\dfrac{1}{2}C_X(U-\hat{U})^2, \text{ output ends 3, 4 are connected.} \end{cases} \tag{16}$$

As a result, the energy storage in the coupling capacitor will decrease to zero when two chaotic PR circuits are synchronized completely. In fact, the field energy flow can be kept in the coupling capacitor, and the capacitance C_X dominates the transport capacity of energy released from the two coupled PR circuits. Therefore, a continuous exchange of field energy can regulate the dynamics of coupled systems effectively. Because of the conservation of energy, the field energy in the coupling capacitor comes from the energy release as H_{CX}=H_1−H_2 in the absence of electromagnetic radiation from these electric devices. The numerical results can be further described to observe the evolution and transport of energy between the coupled systems.

Readers can also extend this study by applying an inductor (induction coil) and memristor between chaotic and hyperchaotic circuits, and interesting results could be confirmed in the forthcoming studies. On the other hand, capacitor coupling just provides insights into field coupling (Guo et al., 2017; Lv et al., 2018; Xu et al., 2018), which is confirmed to benefit signal propagation between neurons even when synapse coupling is suppressed or inactive. Therefore, researchers can build more neural circuits and explore signal encoding and transmission by capacitor and inductor coupling between hyperchaotic circuits. In an experimental method, Ren et al. (2019) confirmed that the synchronization between two Colpitts systems can be realized by building a transformer and that the coupling coefficient of the transformer is an important bifurcation parameter for the synchronization manifold of the system. When field coupling is applied, secure communication can be further investigated using chaos synchronization. The coupling inductor and capacitor can also be used to collect external field energy; for example, electromagnetic radiation energy can be collected by these electric coupling devices and the coupled circuits will be regulated via energy flow.

In fact, we just discussed the case between two nonlinear circuits. The same further investigation becomes attractive and important when field coupling is considered between neurons in a network. As is well known, noise, time delay, and Calcium signal (Tang et al., 2017; Yu et al., 2017) can change the neural activities of neurons. Therefore, neural circuits can be connected via field coupling, and the collective behaviors can be detected for analysis of consensus and synchronization.

4 Conclusions

Based on chaotic PR circuits, symmetric coupling and cross coupling via a single variable are applied to investigate synchronization stability. It was found that symmetric coupling can support the stability of complete synchronization, while cross coupling, for which different channel variables were coupled, just triggers phase synchronization. When a linear resistor is used to activate voltage coupling, complete synchronization is reached while the coupling resistor has to consume a great deal of Joule heat and energy. Complete synchronization failed although phase synchronization can be stabilized when coupling is activated between the outputs from parasitic capacitance C_1, which holds a small capacitance. Complete synchronization, phase synchronization, and anti-phase synchronization can reach the desired target when capacitor coupling is activated, which can build a time-varying electric field, and the energy flow across the coupling capacitor is transmitted to further regulate the outputs and dynamics in the coupled circuits. In summary, capacitor coupling enhances the exchange of energy flow between the coupled circuits; as a result, the synchronization becomes relaxed and no additive energy is consumed as the coupling resistor.

References

Adesnik H, Bruns W, Taniguchi H, et al., 2012. A neural circuit for spatial summation in visual cortex. *Nature*, 490(7419): 226-231. https://doi.org/10.1038/nature11526

Andrievskii BR, Fradkov AL, 2004. Control of chaos: methods and applications. II. Applications. *Autom Remote Contr*, 65(4):505-533. https://doi.org/10.1023/B:AURC.0000023528.59389.09

Balenzuela P, García-Ojalvo J, 2005. Role of chemical synapses in coupled neurons with noise. *Phys Rev E*, 72: 021901. https://doi.org/10.1103/PhysRevE.72.021901

Bao BC, Jiang T, Xu Q, et al., 2016. Coexisting infinitely many attractors in active band-pass filter-based memristive circuit. *Nonl Dynam*, 86(3):1711-1723. https://doi.org/10.1007/s11071-016-2988-6

Bao BC, Jiang T, Wang GY, et al., 2017. Two-memristor-based Chua's hyperchaotic circuit with plane equilibrium and its extreme multistability. *Nonl Dynam*, 89(2):1157-1171. https://doi.org/10.1007/s11071-017-3507-0

Bennett MVL, 1997. Gap junctions as electrical synapses. *J Neurocytol*, 26(6):349-366. https://doi.org/10.1023/A:1018560803261

Bennett MVL, 2000. Electrical synapses, a personal perspective (or history). *Brain Res Rev*, 32(1):16-28. https://doi.org/10.1016/S0165-0173(99)00065-X

Boccaletti S, Farini A, Arecchi FT, 1997. Adaptive synchronization of chaos for secure communication. *Phys Rev E*, 55(5):4979-4981. https://doi.org/10.1103/PhysRevE.55.4979

Budhathoki RK, Sah MP, Adhikari SP, et al., 2013. Composite behavior of multiple memristor circuits. *IEEE Trans Circ Syst I*, 60(10):2688-2700. https://doi.org/10.1109/TCSI.2013.2244320

Burić N, Todorović K, Vasović N, 2008. Synchronization of bursting neurons with delayed chemical synapses. *Phys Rev E*, 78:036211. https://doi.org/10.1103/PhysRevE.78.036211

Buscarino A, Fortuna L, Frasca M, 2009. Experimental robust synchronization of hyperchaotic circuits. *Phys D*, 238(18): 1917-1922. https://doi.org/10.1016/j.physd.2009.06.021

Buscarino A, Fortuna L, Frasca M, et al., 2012. A chaotic circuit based on Hewlett-Packard memristor. *Chaos*, 22(2):023136. https://doi.org/10.1063/1.4729135

Davison IG, Ehlers MD, 2011. Neural circuit mechanisms for pattern detection and feature combination in olfactory cortex. *Neuron*, 70(1):82-94. https://doi.org/10.1016/j.neuron.2011.02.047

Eccles JC, 1982. The synapse: from electrical to chemical transmission. *Ann Rev Neurosci*, 5(1):325-339. https://doi.org/10.1146/annurev.ne.05.030182.001545

Fell J, Axmacher N, 2011. The role of phase synchronization in memory processes. *Nat Rev Neurosci*, 12(2):105-118. https://doi.org/10.1038/nrn2979

Guo SL, Xu Y, Wang CN, et al., 2017. Collective response, synapse coupling and field coupling in neuronal network. *Chaos Sol Fract*, 105:120-127. https://doi.org/10.1016/j.chaos.2017.10.019

Guo SL, Ma J, Alsaedi A, 2018. Suppression of chaos via control of energy flow. *Pramana*, 90(3):39. https://doi.org/10.1007/s12043-018-1534-0

Hahn SL, 1996. Hilbert Transforms in Signal Processing. Artech House, Boston, USA.

Hanias MP, Giannaris G, Spyridakis A, et al., 2006. Time series analysis in chaotic diode resonator circuit. *Chaos Sol Fract*, 27(2):569-573. https://doi.org/10.1016/j.chaos.2005.03.051

He DH, Shi PL, Stone L, 2003. Noise-induced synchronization in realistic models. *Phys Rev E*, 67(2):027201. https://doi.org/10.1103/PhysRevE.67.027201

Ikezi H, deGrassie JS, Jensen TH, 1983. Observation of multiple-valued attractors and crises in a driven nonlinear circuit. *Phys Rev A*, 28(2):1207-1209. https://doi.org/10.1103/PhysRevA.28.1207

Kiliç R, Alçi M, Çam U, et al., 2002. Improved realization of mixed-mode chaotic circuit. *Int J Bifurc Chaos*, 12(6): 1429-1435. https://doi.org/10.1142/S0218127402005236

Kopell N, Ermentrout B, 2004. Chemical and electrical synapses perform complementary roles in the synchronization of interneuronal networks. *PNAS*, 101(43):15482-15487. https://doi.org/10.1073/pnas.0406343101

Li XM, Wang J, Hu WH, 2007. Effects of chemical synapses on the enhancement of signal propagation in coupled neurons near the canard regime. *Phys Rev E*, 76:041902. https://doi.org/10.1103/PhysRevE.76.041902

Louodop P, Fotsin H, Kountchou M, et al., 2014. Finite-time synchronization of tunnel-diode-based chaotic oscillators. *Phys Rev E*, 89:032921. https://doi.org/10.1103/PhysRevE.89.032921

Lv M, Ma J, Yao YG, et al., 2018. Synchronization and wave propagation in neuronal network under field coupling. *Sci China Technol Sci*, in press. https://doi.org/10.1007/s11431-018-9268-2

Ma J, Song XL, Tang J, et al., 2015. Wave emitting and propagation induced by autapse in a forward feedback neuronal network. *Neurocomputing*, 167:378-389. https://doi.org/10.1016/j.neucom.2015.04.056

Ma J, Mi L, Zhou P, et al., 2017. Phase synchronization between two neurons induced by coupling of electromagnetic field. *Appl Math Comput*, 307:321-328. https://doi.org/10.1016/j.amc.2017.03.002

Muthuswamy B, Chua LO, 2010. Simplest chaotic circuit. *Int J Bifurc Chaos*, 20(5):1567-1580. https://doi.org/10.1142/S0218127410027076

Muthuswamy B, Kokate PP, 2009. Memristor-based chaotic circuits. *IETE Tech Rev*, 26(6):417-429. https://doi.org/10.4103/0256-4602.57827

Nazzal JM, Natsheh AN, 2007. Chaos control using sliding-mode theory. *Chaos Sol Fract*, 33(2):695-702. https://doi.org/10.1016/j.chaos.2006.01.071

Neiman A, Schimansky-Geier L, Cornell-Bell A, et al., 1999. Noise-enhanced phase synchronization in excitable media. *Phys Rev Lett*, 83(23):4896-4899. https://doi.org/10.1103/PhysRevLett.83.4896

Parlitz U, Junge L, Lauterborn W, et al., 1996. Experimental observation of phase synchronization. *Phys Rev E*, 54(2): 2115-2117. https://doi.org/10.1103/PhysRevE.54.2115

Pikovsky AS, 1981. A dynamical model for periodic and chaotic oscillations in the Belousov-Zhabotinsky reaction. *Phys Lett A*, 85(1):13-16. https://doi.org/10.1016/0375-9601(81)90626-5

Pikovsky AS, Rabinovich MI, 1978. A simple autogenerator with stochastic behaviour. *Sov Phys Dokl*, 23:183-185.

Pikovsky A, Rosenblum M, Kurths J, 2000. Phase synchronization in regular and chaotic systems. *Int J Bifurc Chaos*, 10(10):2291-2305. https://doi.org/10.1142/S0218127400001481

Qin HX, Ma J, Jin WY, et al., 2014. Dynamics of electric activities in neuron and neurons of network induced by autapses. *Sci China Technol Sci*, 57(5):936-946. https://doi.org/10.1007/s11431-014-5534-0

Ren GD, Zhou P, Ma J, et al., 2017. Dynamical response of electrical activities in digital neuron circuit driven by autapse. *Int J Bifurc Chaos*, 27(12):1750187. https://doi.org/10.1142/S0218127417501875

Ren GD, Xue YX, Li YW, et al., 2019. Field coupling benefits signal exchange between Colpitts systems. *Appl Math Comput*, 342:45-54. https://doi.org/10.1016/j.amc.2018.09.017

Schöll E, Schuster HG, 2008. Handbook of Chaos Control. John Wiley & Sons, Weinheim, Germany.

Song XL, Wang CN, Ma J, et al., 2015. Transition of electric activity of neurons induced by chemical and electric autapses. *Sci China Technol Sci*, 58(6):1007-1014. https://doi.org/10.1007/s11431-015-5826-z

Tang J, Zhang J, Ma J, et al., 2017. Astrocyte calcium wave induces seizure-like behavior in neuron network. *Sci China Technol Sci*, 60(7):1011-1018. https://doi.org/10.1007/s11431-016-0293-9

Timmer J, Rust H, Horbelt W, et al., 2000. Parametric, nonparametric and parametric modelling of a chaotic circuit time series. *Phys Lett A*, 274(3-4):123-134. https://doi.org/10.1016/S0375-9601(00)00548-X

Wang CN, Ma J, Liu Y, et al., 2012. Chaos control, spiral wave formation, and the emergence of spatiotemporal chaos in networked Chua circuits. *Nonl Dynam*, 67(1):139-146. https://doi.org/10.1007/s11071-011-9965-x

Wang CN, Chu RT, Ma J, 2015. Controlling a chaotic resonator by means of dynamic track control. *Complexity*, 21(1): 370-378. https://doi.org/10.1002/cplx.21572

Wu CW, Chua LO, 1993. A simple way to synchronize chaotic systems with applications to secure communication systems. *Int J Bifurc Chaos*, 3(6):1619-1627. https://doi.org/10.1142/S0218127493001288

Xu Y, Jia Y, Ma J, et al., 2018. Collective responses in electrical activities of neurons under field coupling. *Sci Rep*, 8(1):1349. https://doi.org/10.1038/s41598-018-19858-1

Yu WT, Zhang J, Tang J, 2017. Effects of dynamic synapses, neuronal coupling, and time delay on firing of neuron. *Acta Phys Sin*, 66:200201.

Zaher AA, Abu-Rezq A, 2011. On the design of chaos-based secure communication systems. *Commun Nonl Sci Numer Simul*, 16(9):3721-3737. https://doi.org/10.1016/j.cnsns.2010.12.032

Zhang G, Ma J, Alsaedi A, et al., 2018a. Dynamical behavior and application in Josephson junction coupled by memristor. *Appl Math Comput*, 321:290-299. https://doi.org/10.1016/j.amc.2017.10.054

Zhang G, Wu FQ, Hayat T, et al., 2018b. Selection of spatial pattern on resonant network of coupled memristor and Josephson junction. *Commun Nonl Sci Numer Simul*, 65:79-90. https://doi.org/10.1016/j.cnsns.2018.05.018